Available online at www.sciencedirect.com
ScienceDirect
Journal of Power Sources 162 (2006) 41–50
JOURNAL OF POWER SOURCES
www.elsevier.com/locate/jpowsour

Novel composite anode with CO "Filter" layers for PEFC

Chieh-Hao Wan [a,*], Qing-Huang Zhuang [a], Chien-Heng Lin [a], Meng-Tsun Lin [a], Chihhsiong Shih [b]

[a] *Institute of Materials and System Engineering, MingDao University, Changhua, Taiwan*
[b] *Department of Computer Science and Informational Engineering, Tunghai University, Taiwan*

Received 28 April 2006; received in revised form 21 June 2006; accepted 22 June 2006
Available online 27 July 2006

Abstract

This study proposes a novel anode catalyst layer structure to improve the CO tolerance and cell performance. A layered structure is composed of an outer and an inner catalyst layer. The outer catalyst layer acts as a CO barrier and consists of a nano Ru/Pt layer (0.06 mg cm^{-2}) deposited by magnetron sputtering and a Pt_{50}–Ru_{50} layer (0.10 mg cm^{-2}) applied by screen-printing to the GDL. The inner catalyst layer is a pure Pt layer (0.07 mg cm^{-2}) produced by a direct-printing method onto the PEM. The roles of outer and inner catalyst layers which improve the CO tolerance and cell performance are investigated in this paper. SEM, X-ray, EDS and EPMA analyses were used to characterize microstructures, phases, chemical composition and distributions of the obtained electrocatalyst layers. Hydrogen containing 50 ppm CO is continuously fed to the anode side to investigate the relationships. The MEAs consist of a Nafion 117 membrane and a commercial electrocatalyst (20% Pt/C from E-TEK) on the cathode side. The results demonstrate that this proposed anode catalyst layer structure exhibits a superior performance and CO tolerance capability in pure hydrogen and CO containing hydrogen fuels. The improved CO tolerance capability is attributed to the filtering effect of the outer catalyst layer.

Keywords: Novel anode catalyst layer structure; Filtering effect; CO tolerance capability; Deposited nano Ru/Pt layer; PEFC

1. Introduction

The polymer electrolyte fuel cell (PEFC) has great potential for mobile and stationary powering applications. Such systems operate at high efficiencies when using pure hydrogen, but can fail when using hydrogen derived from hydrocarbon or methanol processing. The reason for this failure is the presence of CO in the reformed gas (0.01–2%) which poisons the Pt electrocatalyst in the anode. Adsorbed CO not only affects the reactivity of the accessible electrode surface by preventing H_2 adsorption by site exclusion, but also lowers the reactivity of the remaining uncovered sites through dipole interactions and electron capture. Much attention has been devoted to development of a non-noble metal electrocatalyst in the last decades for replacing the platinum catalyst in PEFC and other low temperature fuel cells. However, platinum remains the best candidate [1].

In order to overcome the CO poisoning problem in PEFCs, many solutions have been developed. One solution to mitigating the poisoning is to use alloy catalysts such as Pt–Ru, Pt–Mo, Pt–Ru–Mo, Pt–Sn, Pt–Ru–Wo_3 and Pd–Au, which have improved CO tolerance [2–13]. The improvement is due to either a lowered CO oxidation potential or a weakened adsorption of CO on these catalysts. This is the most convenient approach because it does not introduce any additional steps or hardware. However, the alloyed catalysts such as Pt–Ru alloy are not as active as Pt when pure hydrogen is the fuel [1]. Another solution is to bleed very low levels of oxidant into the fuel feed stream, for instance, O_2 [14,15] or H_2O_2. However, even the addition of high levels of O_2 to the feed stream (2–4% by volume of hydrogen) provides only approximately a 100 ppm CO tolerance. Roughly one out of every 400 O_2 molecules participates in the oxidation of CO, with the balance reacting with hydrogen [16]. The remaining oxygen chemically combusts with hydrogen. The combustion reaction not only lowers the fuel efficiency, but might also accelerate the sintering of catalyst particles to lead to a performance decline with time. The placement of a layer of Ru catalyst in front of the Pt electrode to act as a filter has been

* Corresponding author. Tel.: +886 4 8890445; fax: +886 4 8890445.
E-mail address: chiehhao@mdu.edu.tw (C.-H. Wan).

0378-7753/$ – see front matter © 2006 Elsevier B.V. All rights reserved.
doi:10.1016/j.jpowsour.2006.06.074

shown to increase the effectiveness of the oxygen addition over a conventional Pt–Ru alloy catalyst [17]. This method also eliminates the process of alloying the Pt and Ru metals. In the work of Huag et al. [18], the sputter-deposited Ru filter anodes consisting of one Ru layer and three Ru layers separated by Nafion-carbon ink are compared to Pt, Pt–Ru alloy and an ink-based Ru filter anode in CO tolerance capability and cell performance. For an anode feed consisting of hydrogen, 200 ppm CO, and 2% O_2 (in the form of an air bleed), all the Ru filter anodes outperformed the Pt–Ru alloy. Huag et al. [18] also suggested that the CO tolerance of the electrode could be further improved by reducing the amount of Ru on each layer and the thickness of each Nafion-carbon ink layer to a monolayer.

Compared with new electrocatalyst development, the improvement of electrode structure could be much more attractive for PEFC commericalization. Yu et al. [19] have proposed a composite anode for a CO tolerant PEFC. The anode electrode structure is designed to make the poisonous CO react in a separate layer with a CO active electrocatalyst (Pt–Ru alloy) in advance, and thus make the main hydrogen to react at another layer using a traditional platinum electrocatalyst. The modified electrode shows excellent cell performance and CO tolerance with a reduced noble metal loading.

The objective of this work is to improve the CO tolerance and cell performance through the proposed multi electrocatalytic layer prepared by the magnetron sputtering deposition and direct-printing techniques. The proposed catalyst layer structure is shown in Fig. 1(D). This structure is obtained by depositing a Ru/Pt layer by magnetron sputter deposition on a printed Nafion-carbon ink layer, followed by screen-printing a Pt_{50}–Ru_{50} layer in order to attain the required three-dimensional reaction zone for the CO barrier. The actual reaction zone of the hydrogen fuel occurs at the direct-printed Pt layer on the PEM anode. We compared the electrode performance and CO tolerance of the proposed catalyst layer structure to structures of Pt, Ru/Pt, and conventional Pt_{50}–Ru_{50} structure anodes (as shown in Fig. 1(A)–(C)). The roles of the outer and inner catalyst layer relating to the enhancements in cell performance and CO tolerance are also investigated.

2. Experiment

Fig. 1 shows the four types membrane electrode assembly (MEA) in this study. The difference between them is the anode catalyst layer. The anode catalyst layer shown in Fig. 1(A) is obtained by depositing a Ru/Pt layer by magnetron sputter deposition on a printed Nafion-carbon ink layer sandwitched alternatively together in three repetitions, and the substrate is the gas diffusion layer in order to attain the required three-dimensional reaction zone. This structure is considered to be the structure (I) catalyst layer. The corresponding sample is II-A and II-C MEA, and the anode loadings were 0.08 and 0.30 mg cm^{-2}, respectively (as shown in Table 2). The anode catalyst layer exhibited in Fig. 1(B) is similar to that of the structure (I) catalyst layer. The only difference between them is the sputter-deposited Pt layer. This structure is regarded as structure (II) catalyst layer and the corresponding sample is I-C MEA. The anode loading is 0.15 mg cm^{-2} (as shown in Table 2). Fig. 1(C) shows the anode catalyst layer prepared by screen-printing a single Pt_{50}–Ru_{50} layer on the GDL. There is no sputter-deposited layer. This is a conventional structure and referred to as structure (III) catalyst layer. The corresponding sample is an ink-based MEA. The anode loading of this MEA is 0.23 mg cm^{-2}. The anode catalyst layer shown in Fig. 1(D) combines a deposited Ru/Pt layer (loading is 0.06 mg cm^{-2}) and a printed Pt_{50}–Ru_{50} layer (loading is 0.10 mg cm^{-2}) on the GDL, and a Pt direct-printing layer (loading is 0.07 mg cm^{-2}) on the PEM. This structure is regarded as structure (IV) catalyst layer. The corresponding sample is IV MEA and the anode loading is 0.23 mg cm^{-2} (as shown in Table 2). The anode Pt loadings of the IV MEA, II-C MEA and I-C MEA are same, while the anode Pt loading of the ink-based MEA approximates to that of the IV MEA, i.e. 0.12 mg cm^{-2}. On the other hand, the cathodes of all the MEAs were prepared by printing a Pt catalyst layer onto the GDL. Table 2 lists the cathode loadings for all the studied MEAs and the magnitude is around 0.25 mg cm^{-2}.

A 5 wt.% Nafion solution in H^+ form supplied by DuPont, Inc., USA, is used as the proton conductive agent in the catalyst layer. A 50% wet proof carbon cloth is used as the gas diffusion layer. Twenty weight percent of Pt on Vulcan XC-72 (20% Pt/C) served as the electrocatalyst for the cathode electrode (E-TEK Division of De Nora, Inc., USA). The 20% Pt_{50}–Ru_{50}/C supplied by the E-TEK Division of De Nora, Inc., USA is adopted as the electrocatalyst for the anode of the ink-based MEA .The carbon powder used for the backing layer is Vulcan XC-72. HPLC grade solvents are used for the preparation of the catalyst slurry. The fabrication processes of the electrodes and the MEAs as well as the measurement procedures of the polarization curves for various MEAs are illustrated as below.

2.1. Preparation of catalyst layer with multi Pt layer

Nafion-carbon ink layer (NCL) is prepared by first mixing an appropriate amount of isopropanol or *n*-butyl acetate with Vulcan XC-72 carbon powders in a 60 ml reactor for 1 h. The required amount of the Nafion solution is then added and mixed until the homogenous mixture is obtained. An appropriate amount of solvent is removed to obtain the Nafion-carbon ink. Both sides of the carbon cloth are printed with the Nafion-carbon ink using a screen-printing method and then dried in the oven at 140 °C for 2 h. The carbon cloth with a Nafion-carbon ink layer is placed on the holder designed by the author in the sputtering chamber and the chamber pressure is pumped to reach 266.6 mPa. The insulation between the Pt target and chamber body should be good before starting the sputtering process. Before turning on the target power supply to reach 0.25 A, argon gas is introduced to the chamber until the required pressure is reached. The Pt or Ru deposition rates and the corresponding process parameters are listed in Table 1. Note that the thickness of the printed Nafion-carbon ink layer is approximately 2 μm.

Multi Pt catalyst layer electrodes were prepared by first screen-printing the gas diffusion layer (GDL) with the Nafion-

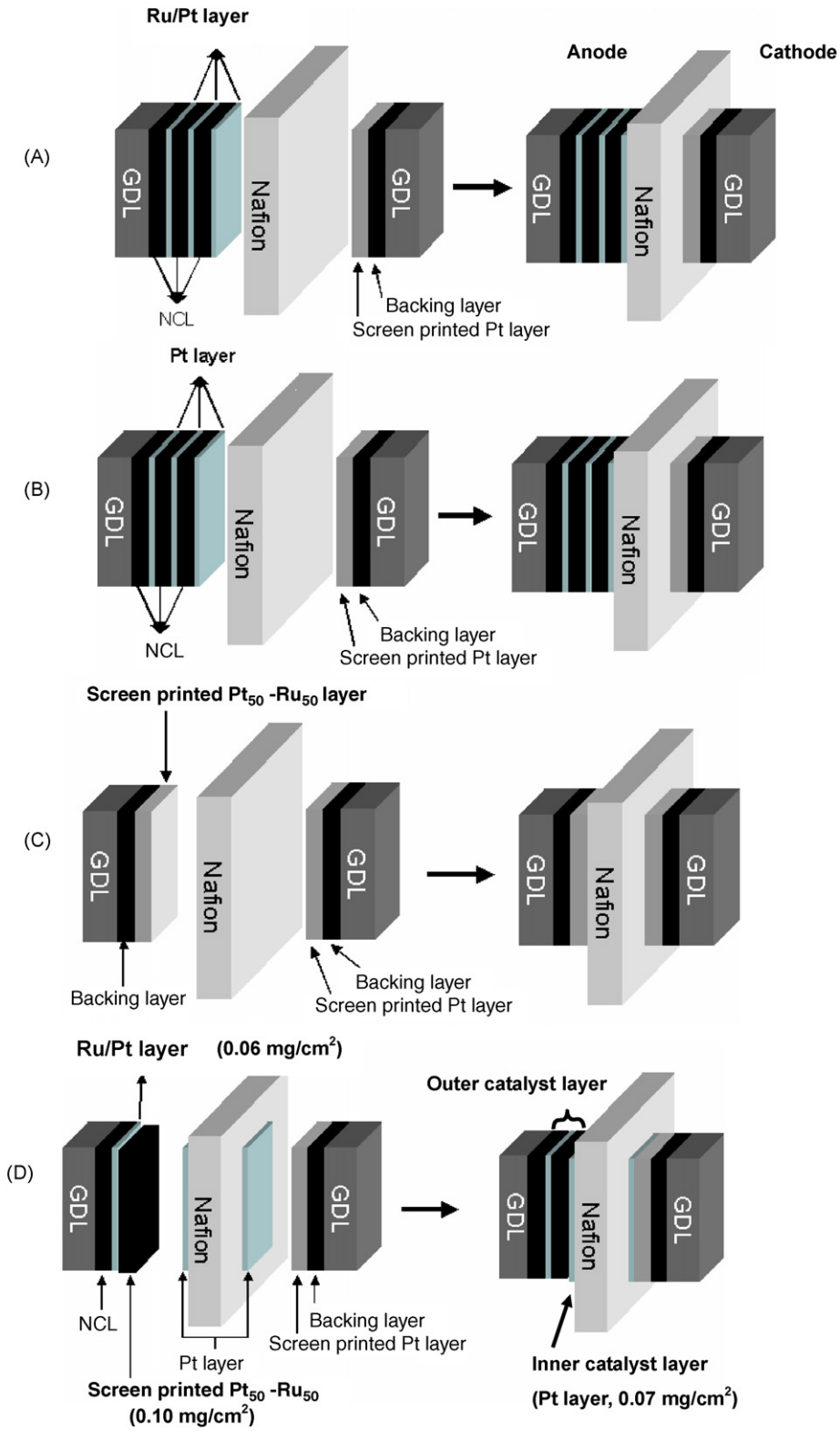

Fig. 1. Diagrams of studied anode catalyst layer structure and MEAs: (A) structure (I) catalyst layer; (B) structure (II) catalyst layer; (C) structure (III) catalyst layer; (D) structure (IV) catalyst layer.

carbon ink. The electrode was then subjected to a vacuum of 266.6 mPa before the appropriate catalyst was sputter deposited. An appropriate amount of Nafion solution was impregnated into the deposited Pt layer using a brushing method. This sequence was repeated until the desired number of layers were achieved. The amount of the Pt loading was controlled by the sputtering time and loadings are listed in Table 2. The top-view SEM images show the surface characteristics of the film.

Table 1
Process parameters and resulted Pt or Ru loadings in this study

Sample code	Process parameters				Pt or Ru loading ($mg\,cm^{-2}$)	Depositing rate ($mg\,s^{-1}\,cm^{-2}$)
	Bias voltage (V)	Pt or Ru target current (A)	Pressure (Torr)	Sputtering time (s)		
SP–Pt	0	0.25	2×10^{-2}	60	0.112	1.86×10^{-3}
SP–Ru	0	0.29	2×10^{-2}	90	0.103	1.14×10^{-3}

2.2. Preparation of catalyst layer with multi Ru/Pt layer

The preparation of a multi Ru/Pt catalyst layer electrode is similar to that of the multi Pt catalyst layer electrode. The only difference is that we deposited a thin layer of Ru followed by a Pt catalyst layer in the required amount. An appropriate amount of Nafion solution was impregnated on the deposited Ru/Pt layer using a brushing method. This sequence was repeated until the desired number of layers were achieved. The amounts of the deposited Ru and Pt elements on the electrode were controlled by the sputtering time. Table 2 shows the loadings obtained.

2.3. Preparation of ink-based electrodes by the screen-printing method

The preparation of a catalyst ink for the ink-based electrode is similar to that of the Nafion-carbon ink. The only difference is that we used a 20% Pt_{50}–Ru_{50}/C electrocatalyst instead of Vulcan XC-72 carbon powders. The side face of the carbon cloth with backing layer was put under the halftone and an appropriate amount of catalyst ink was placed on the halftone. An active catalyst layer was obtained after the catalyst ink was smeared smoothly by squeegee onto the carbon cloth and dried at 135 °C under ambient pressure for 2–3 h. The resulted loadings are shown in Table 2.

2.4. Preparation of the structure (IV) electrode

The structure IV electrode was prepared by first screen-printing the GDL with the Nafion-carbon ink. The electrode was then subjected to a vacuum of 266.6 mPa before the appropriate Ru/Pt catalyst was sputter deposited. An appropriate amount of Nafion solution was impregnated on the deposited Ru/Pt layer using the brushing method. The catalyst ink for the ink-based electrode was screen-printed onto the surface of the deposited Ru/Pt layer. The production of a directly printed Pt layer on the PEM adopted the method of Hsu and Wan [20] by using a 20% Pt/C as the electrocatalyst. Hot pressing of the GDL electrode and PEM containing Pt layer form the electrode and MEA of structure IV. The resulting loadings of the deposited Ru/Pt layer, screen-printing Pt_{50}–Ru_{50} layer and direct-printing Pt layer are 0.06, 0.10 and 0.07 $mg\,cm^{-2}$, respectively.

2.5. Preparation of cathode electrode by screen-printing method

The preparation of the catalyst ink for the cathode was similar to that of the Nafion-carbon ink. The only difference was that we used a 20% Pt/C electrocatalyst instead of Vulcan XC-72 carbon powders. The side face of the carbon cloth with backing layer is put under the halftone and an appropriate amount of catalyst ink was placed on the halftone. An active catalyst layer was obtained after the catalyst ink was smeared smoothly by a squeegee on the carbon cloth and dried at 135 °C under ambient pressure for 2–3 h. The catalyst layer for the cathode of the structure IV MEA was a combination of the catalyst layer on the PEM and GDL. The cathode loading obtained was 0.25 $mg\,cm^{-2}$.

2.6. Preparation of the membrane electrode assembly (MEA)

Nafion 117 (DuPont, Inc., USA) was used as the polymer electrolyte membrane. Prior to its use, each membrane was first boiled in 3–5% hydrogen peroxide, then washed with water, and then boiled in diluted sulfuric acid. Finally, it was washed with deionized water. The PEM prior to hot pressing was brushed with an appropriate amount of Nafion solution on both sides of the reactive surface area (5 cm^2). The PEM was then placed between the two electrodes and MEA was obtained by applying a force of 3450–4200 kg_f at 135 °C for 2 min.

2.7. Evaluation of the electrode/MEA

The MEA was placed between two silicone gaskets of thickness 0.24 mm and inserted between two graphite plates with serpentine grooves, and then placed in a single cell test fixture (5 cm^2) supplied by Electrochem, Inc., USA. A uniform torque of 80 $kg_f\,cm$ was applied onto the eight bolts that were used to assemble the PEFC. The fuel cell was connected to the test station (Fuel cell technologies, Inc., USA) that was equipped

Table 2
Characteristics of MEAs used in this study

Sample code	Anode ($mg\,cm^{-2}$)	Cathode ($mg\,cm^{-2}$)
IV	0.23 (combination of sputtering and printing)	0.25 (prepared by printing method)
Ink-based	0.23 (printing one layer Pt_{50}–Ru_{50})	0.25 (prepared by printing method)
II-C	0.30 (sputtering three layers Ru_{48}/Pt_{52})	0.25 (prepared by printing method)
II-A	0.08 (sputtering three layers Ru_{48}/Pt_{52})	0.25 (prepared by printing method)
I-C	0.15 (sputtering three layers Pt)	0.25 (prepared by printing method)

with a gas humidifier, a mass flow controller, and a temperature indicator controller. Humidified hydrogen/hydrogen containing 50 ppm CO and oxygen gases were fed into the cell at a flow rate of 100 and 200 cc min^{-1}, respectively. The humidifier temperature for anode and cathode were set to a value that could complete the humidification of anode and cathode gas streams for all trials. We evaluated the current–voltage (*I–V*) characteristics of the cell at various temperatures and pressures as mentioned. When the MEA was tested in the hydrogen containing 50 ppm CO fuel, the poisoned anode was recovered by using pure O_2 for 35 min until the performance was redeemed to the un-poisoned state.

The cyclic voltammetric method was employed using a potentiostat (EG&G model-263A, Princeton Applied Research, USA). Cyclic voltammograms (CV) were recorded for the electrodes during which an atmosphere of argon gas was maintained on the test electrode side, while that of H_2 was maintained on the counter electrode side. The CVs were recorded between −0.1 and 1.4 V at 50 mV s^{-1}. These experiments were carried out to determine the EASA of the electrodes. The EASA were obtained using a procedure previously reported [21,22].

3. Results and discussion

3.1. Microstructure and morphology of the anode catalyst layer

Table 2 lists the loadings and the specific characteristics for the anode and cathode that formed the MEAs in this study. Fig. 2(A) is the SEM picture for the printed Nafion-carbon ink layer of the anode of II-A and II-C MEA. The printed layer contains the Nafion ionomer and electron conductive carbon particles. The Nafion-carbon ink layer shows the porous honeycomb-like microstructure. The surface microstructure of the third deposited Ru/Pt layer for the anode of II-A MEA is shown in Fig. 2(B). The sputtering time of Ru and Pt elements are 13 and 8 s, respectively. The extent of the sputtering time for the Ru and Pt elements were 43 and 27 s in Fig. 2(C). This was the surface microstructure of the third deposited Ru/Pt layer for the anode of II-C MEA. The observed particle size was apparently larger than that of the deposited Ru/Pt layer for the anode of II-A MEA. In Fig. 2(D), we clearly observe the particle size between 50 and 80 nm and this particle was a cluster. Accordingly, the particle size for those of the anode of II-A MEA was smaller than 50–80 nm. In order to confirm the composition of these cluster particles layers, we used a grazing incident X-ray diffraction (GID) method to obtain the X-ray diffraction pattern at an X-ray incident angle of 1°. Fig. 3(A) shows the X-ray diffraction pattern of the third deposited Ru/Pt layer of the anode of II-C MEA. The small peak located at 36.9° is the characteristic peak of the Ru (2 0 1) face. The strong sharp peak position at 39.5° is the diffraction peak of the Pt (1 1 1) face, while the broadened peak at 78.9° is the diffraction peak of the Pt (3 1 1) face. The diffraction peak of the Ru is not obvious. This is because the intrinsic intensity of the Ru element diffraction peak is relatively low and the peak position is close to that of Pt. In addition, the amount of deposited Ru with the mentioned process parameters is relatively low, i.e. 0.05 mg cm^{-2}, and Ru layer is partially covered by a Pt layer. Based on the X-ray data, the cluster particles layer

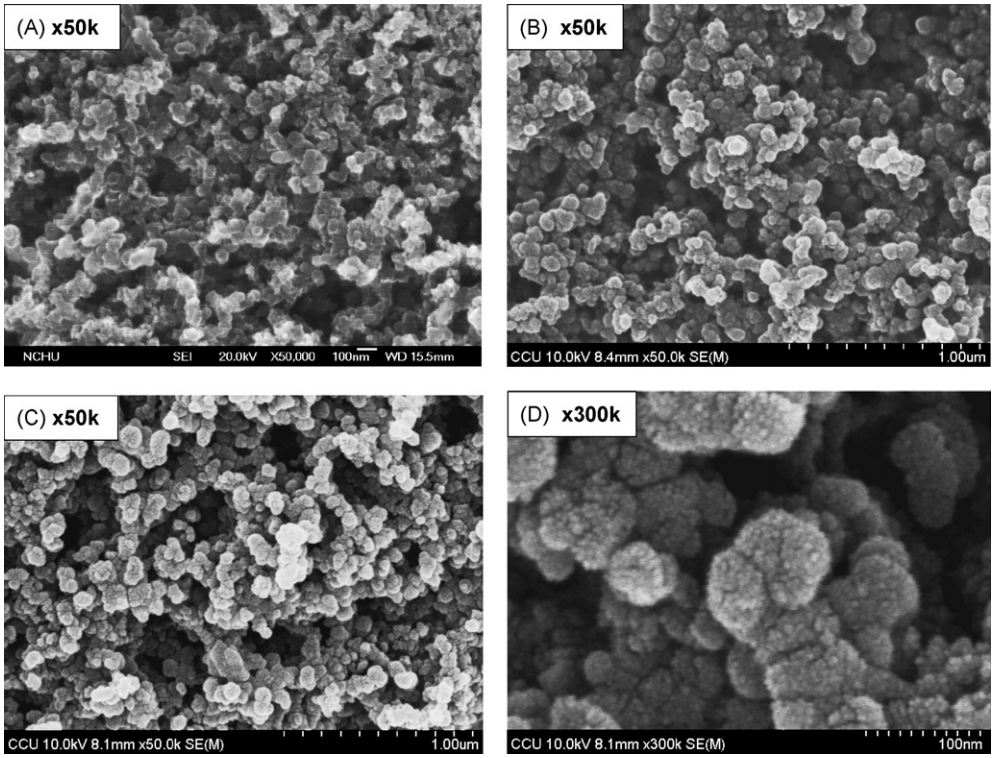

Fig. 2. SEM images for: (A) NCL layer; (B) the third deposited Ru/Pt layer of II-A MEA; (C) the third deposited Ru/Pt layer of II-C MEA; (D) the third deposited Ru/Pt layer of II-C MEA at 300,000×.

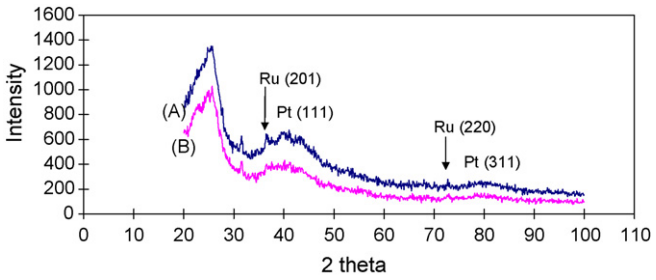

Fig. 3. X-ray diffraction patterns for: (A) the third deposited Ru/Pt layer of II-C MEA and (B) the third deposited Pt layer of I-C MEA.

contains Ru and Pt phases rather than an Pt–Ru alloy phase. EPMA analysis was used to examine the composition percentage of Ru and Pt elements on the surface. The results indicate that the atomic ratio of Pt and Ru is approximately 52:48. EDS analysis shows the same atomic ratio, indicating the distribution of Pt and Ru elements on the surface was around 52:48. This further confirms that the nanocluster layer consists of well dispersed Pt and Ru elements. According to the results of the SEM, X-ray, EPMA and EDS, we suggest the most likely distribution of deposited Pt and Ru elements in Fig. 4. The Ru element is firstly deposited on Nafion-carbon ink layer (NCL) and grown to form a nanocluster. These nanoclusters are well dispersed on the NCL. Deposited Pt either is attached to the Ru cluster or forms a cluster by itself. The deposited Pt subsequently grows to a nanocluster with a particle size of 50–80 nm. Consequently, the resulting nanocluster layer consists of pure Ru, mixed Ru/Pt and pure Pt clusters in which the pure Ru cluster is partially distributed under the cluster layer. In other words, the nano Ru cluster partially locates at the outer catalyst layer.

In order to obtain the thickness of the deposited Ru/Pt layer, a piece of single crystal silicon wafer with a smooth surface was placed on the same holder with the same sputtering conditions as the GDLs for the sputtering time of Ru element for 60 s and of Pt element for 30 s, respectively. The resulting Ru and Pt loadings were 0.068 and 0.056 mg cm^{-2}. The resultant Ru–Pt/SiO_2 stack was subjected to a cross-sectional SEM imaging to verify the sputter-deposited film thickness. The resultant thickness was approximately 70 nm. Therefore, the sputtering thickness increase rate was around 46.6 nm min^{-1} (the time is the sum of sputtering time for the Ru and Pt elements). On the basis of this data, we can infer the thickness of each deposited Ru/Pt layer to be around 54 nm for the anode of II-C MEA. Consequently, the thickness of each deposited Ru/Pt layer for the anode of II-A MEA is expected to be 16 nm. Note that due to the higher roughness of carbon layer than that of the single crystal silicon wafer, the actual thickness of the deposited Ru/Pt layer on the carbon layer is less than the one on the silicon wafer.

The anode catalyst layer structure of I-C MEA is similar to that of structure (I) catalyst layer. The only difference between them is the sputter-deposition layer, which is a pure Pt layer for the anode of I-C MEA. The surface microstructure of the deposited Pt layer is similar to those shown in Fig. 2(C). The resultant Pt particle size is approximately 50–80 nm. Fig. 3(B) shows the X-ray diffraction pattern obtained at the X-ray incident angle of 1° for the third deposited Pt layer of the anode of I-C MEA. The characteristic peaks of Pt [23] are clearly observed at a 2θ of 39.5° and 79.1°. These two peaks exhibit a broadened shape and a relatively low intensity. EPMA results further confirm that the composition of the nanocluster is Pt. The result of EDS analysis indicates that the Pt is well distributed on the surface. The thickness of deposited Pt layer is determined by the method previously stated. The obtained sputtering thickness increase rate was 35 nm min^{-1}. On this basis, we can infer the thickness of each deposited Pt layer to be around 15.7 nm for the anode of I-C MEA. Summarizing the above results, we know that each deposited catalyst layer at the anode of I-C MEA is formed by a well-distributed Pt cluster of particles on the NCL.

The anode catalyst layer of IV MEA is composed of a deposited Ru/Pt layer with the same sputtering condition to the anode catalyst layer of II-C MEA, a screen-printing Pt_{50}–Ru_{50} layer on GDL, and a direct-printing Pt layer on PEM. Due to the same sputtering conditions, the microstructure and composition distribution of each deposited Ru/Pt layer were similar to that of the II-C MEA (as shown in Fig. 4). This deposited Ru/Pt layer thickness was 32 nm. The microstructure of the screen-printing Pt_{50}–Ru_{50} layer was the same as in the image shown in Fig. 2(A), i.e. a porous honeycomb-like structure. The direct-printing Pt layer on PEM has a similar microstructure. The thickness of the screen-printing layer was about 6 μm, while the direct-printing Pt layer was only 1 μm, which was measured by calipers. Therefore, the anode thickness of the IV MEA was approximately 10 μm.

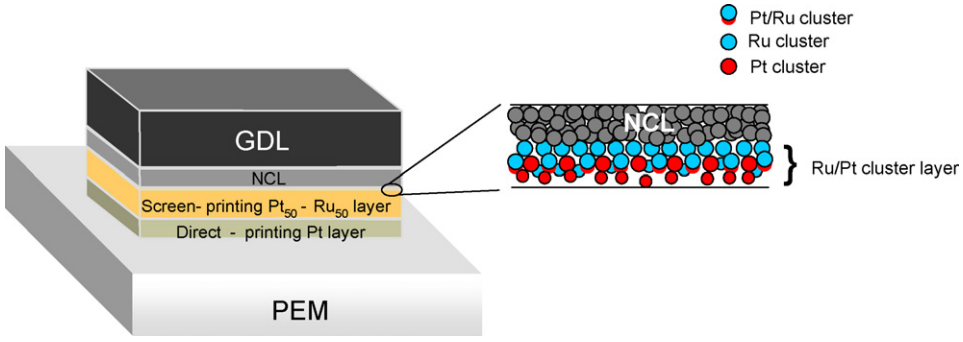

Fig. 4. Schematic of deposited nano Ru/Pt catalyst layer.

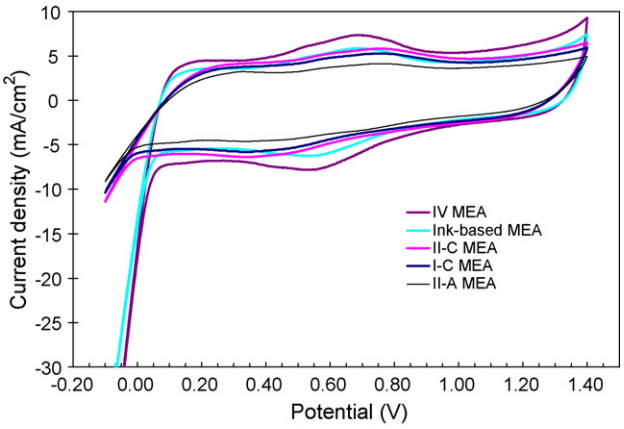

Fig. 5. *I/V* profiles of the studied MEAs.

3.2. Electro-active surface area (EASA) for the studied anode

The EASA of our proposed anode is measured using the cyclic voltammetric method and the representative *C/V* profiles are shown in Fig. 5. Data for the EASA ($m^2\,g^{-1}$ Pt) are listed in Table 3. Cyclic voltammetric studies from 0.0 to 0.4 V provide information on the hydrogen adsorption and desorption which occurs on the platinum surface. The region from 0.4 to 0.5 V is regarded as the double-layer region [22]. To evaluate the Pt surface area, the current densities of hydrogen adsorption and desorption were integrated separately and referred to a charge of 210 $\mu C\,cm^{-2}$, which corresponds to a monolayer of hydrogen adsorption on the Pt surface [24]. Apparently, the IV MEA had the largest integrated area, followed by the II-C MEA, I-C MEA, ink-based MEA and II-A MEA. The IV MEA, II-C MEA and I-C MEA had the same anode Pt loading of 0.15 $mg\,cm^{-2}$, and the anode Pt loading of the ink-based MEA was close to that of IV MEA, i.e. 0.12 $mg\,cm^{-2}$. Thus, the true reactive surface area follows the sequence of IV MEA > ink-based MEA ≈ I-C MEA ≈ II-C MEA > II-A MEA (as shown in Table 3). This indicates that the proposed IV MEA gains the highest EASA though it has the highest anode Pt loading, i.e. 84.53 $m^2\,g^{-1}$ Pt, while the anode with deposited catalyst layers for the I-C MEA and II-C MEA show almost the same EASA as that of the ink-based MEA. Accordingly, we can infer that the sequence of performance is the same as that of the EASA for the studied MEAs. The current density (at 0.60 V) listed in Table 3 confirms this. Note that the EASAs for the four samples with the mentioned catalyst layer structure were rather similar

Table 3
Current density and EASA of the studied MEAs

Sample code	Current density at 0.6 V ($mA\,cm^{-2}$)	EASA ($m^2\,g^{-1}$ Pt)
IV	554.5	84.53
Ink-based	496.4	83.15
II-C	474.2	83.07
II-A	174.6	81.64
I-C	447.2	83.12
IV (0 kPa)	422.0	–

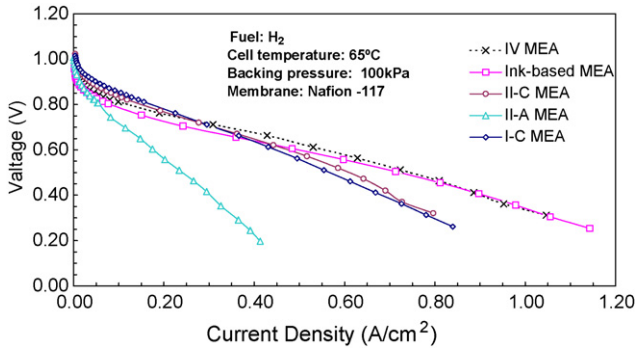

Fig. 6. Polarization curves for various MEAs fed with pure H_2 fuel operated at 65 °C (cell temperature) and 100 kPa (backing pressure).

to or larger than that of the E-TEK product (81.67 $m^2\,g^{-1}$ Pt) [20].

3.3. Performance of the MEAs using pure hydrogen as fuel

The polarization curves exhibited in Fig. 6 were obtained by using pure H_2 as the anode fuel at a cell temperature of 65 °C under a backing pressure of 100 kPa. Obviously, the IV MEA had the best cell performance, followed by ink-based MEA, II-C MEA, I-C MEA and II-A MEA. The current density at a voltage of 0.6 V shown in Table 3 further confirms this. In summary, the IV MEA possesses higher cell performance than ink-based MEAs. This result implies that the performance for the proposed anode structure is superior to that of a conventional structure with pure H_2.

3.4. Performance of MEAs using hydrogen containing 50 ppm CO as fuel

In order to understand the CO tolerance of the studied MEAs, we supplied hydrogen containing 50 ppm CO as the anode fuel to test the performance of the MEAs. Fig. 7 shows the polarization curves obtained after 5 min of hydrogen fuel containing 50 ppm CO. We use solid symbols to represent the polarization curves obtained at a cell temperature of 40 °C with a 100 kPa backing pressure. The hollow symbols represent the polarization curves

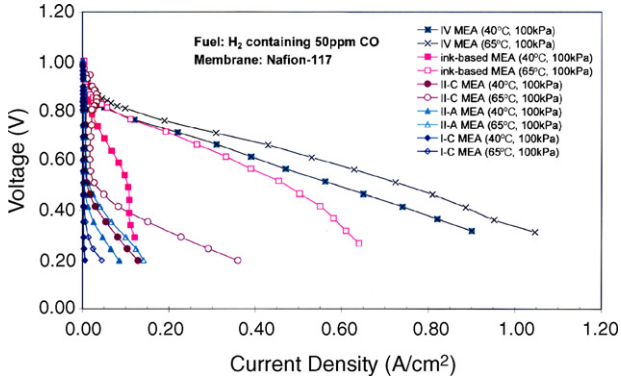

Fig. 7. Polarization curves for various MEAs obtained after 5 min of the H_2 fuel supply containing 50 ppm CO at the indicated cell temperatures and backing pressures.

measured at the cell temperature of 65 °C under the same backing pressure. The sequence of CO tolerance capability for the studied MEAs is as follows: IV MEA > Ink-based MEA > II-C MEA > II-A MEA > I-C MEA. CO tolerance capability is better at higher temperatures. Comparing the polarization curves obtained from the anode feed of pure H_2 and hydrogen containing 50 ppm CO fuel, we find that the I-C MEA without Ru has better performance and utilization efficiency of the catalyst (2.981 A mg^{-1} Pt at 0.6 V) in the pure hydrogen fuel but performs very poorly in hydrogen containing 50 ppm CO fuel (almost no current). By contrast, the II-C MEA that contains Ru exhibits comparatively good tolerance towards CO. Even though the II-A MEA contained the lowest amount of Ru element in the anode, the catalyst layer still had some degree of CO tolerance. This indicates that the existence of Ru in the catalyst layer has indeed improved the CO tolerance. Better CO tolerance ability is achieved by increasing the content of Ru in the catalyst layer. This result is consistent with the literature [19]. Yu et al. [19] indicates that the anode loading for efficient CO tolerance was 0.28 mg Pt–Ru cm^{-2} plus 0.02 mg Pt cm^{-2}. Consequently, the IV MEA and ink-based MEA, which have the same anode loadings of 0.23 mg cm^{-2}, posses better CO tolerance than the other MEAs.

We continuously fed the hydrogen containing 50 ppm CO fuel to the anode side to investigate the dependence of CO tolerance ability over time for the MEAs. Fig. 8 exhibits the polarization curve variations with time for the IV MEA at a cell temperature of 65 °C under a backing pressure of 100 kPa. Apparently, the electrode performance remains unchanged after 3 h and declines to 81.5% after 5 h compared to the electrode performance in pure hydrogen. The corresponding current densities for 3 and 5 h were 510.3 and 415.6 mA cm^{-2} (at 0.60 V), respectively. Fig. 9 presents the polarization curves with time for the ink-based MEA at the same cell temperature and backing pressure to that of the IV MEA. The performance declined drastically to 29 and 78% of the MEA running on pure hydrogen fuel in 5 and 15 min, respectively. The corresponding current densities for 5 and 15 min were 345.1 and 102.0 mA cm^{-2} (at 0.60 V), respectively. It is clear that the proposed anode catalyst layer structure has superior CO tolerance. At the same cell temperature and backing pressure, the electrode performance for the II-C MEA drops to less than 90% of the MEA running on pure hydrogen fuel when 50 ppm CO is added to the hydrogen feed stream (Fig. 10). The CO poisoning rate for II-C MEA is obviously much higher than that of ink-based MEA and IV MEA, indicating the catalyst in the anode of II-C MEA is instantly poisoned. The II-A and I-C MEA even have a larger poisoning rate than the II-C MEA. Especially, the Ru element free I-C MEA (as shown in Figs. 11 and 12) shows an extremely fast poisoning rate.

Comparing the CO poisoning rate between the II-C and I-C MEA that comprise of a deposited nano Ru/Pt or Pt layer and the ink-based MEA, we find that the poisoning rate for

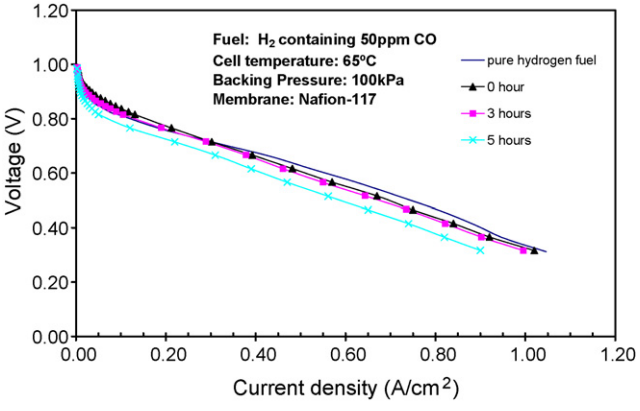

Fig. 8. Polarization with time for the IV MEA using H_2 containing 50 ppm CO fuel at 65 °C (cell temperature) and 100 kPa (backing pressure).

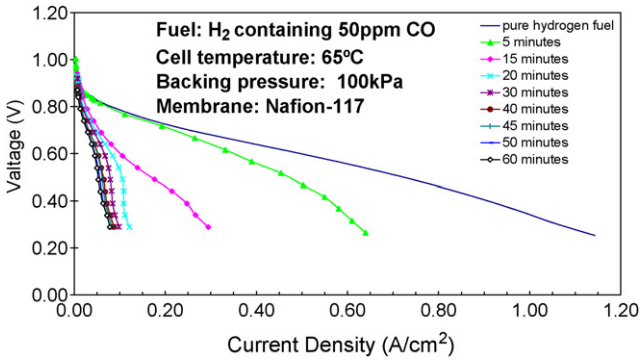

Fig. 9. Polarization with time for the ink-based MEA using the H_2 containing 50 ppm CO fuel at 65 °C (cell temperature) and 100 kPa (backing pressure).

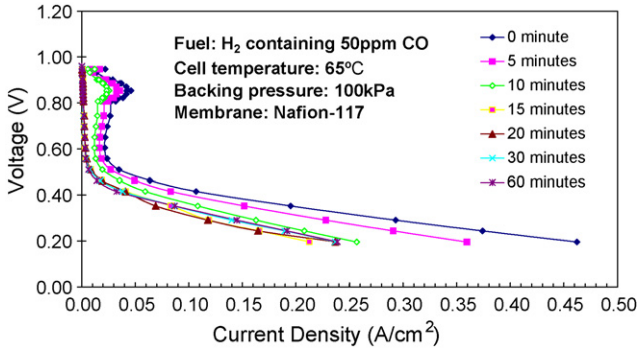

Fig. 10. Polarization with time for the II-C MEA using H_2 containing 50 ppm CO fuel at 65 °C (cell temperature) and 100 kPa (backing pressure).

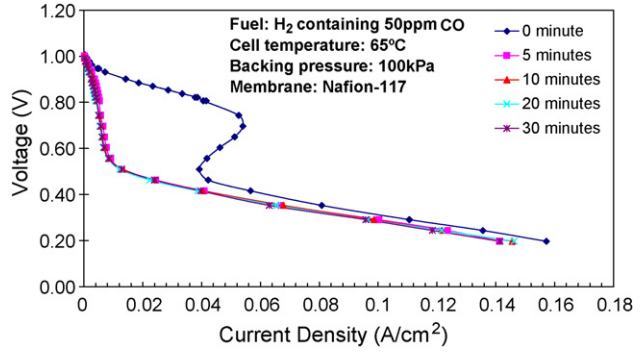

Fig. 11. Polarization with time for the II-A MEA using H_2 containing 50 ppm CO fuel at 65 °C (cell temperature) and 100 kPa (backing pressure).

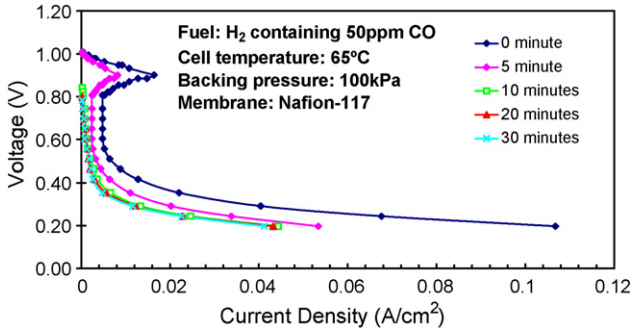

Fig. 12. Polarization with time for the I-C MEA using H_2 containing 50 ppm CO fuel at 65 °C (cell temperature) and 100 kPa (backing pressure).

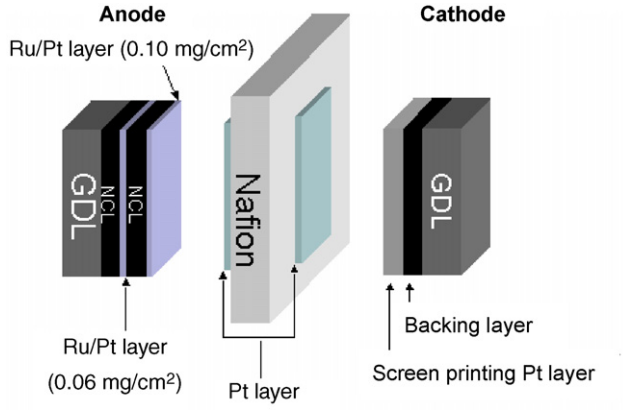

Fig. 14. Diagram of the V MEA with two deposited nano Ru/Pt layers as the outer catalyst layer at anode.

the former were extremely fast, while the latter were relatively slow (as shown in Figs. 7 and 9–12). From the viewpoint of reaction kinetics, the contact surface area between the catalyst and reactants is a key factor to influence the reaction rate. The surface area of deposited nano Ru/Pt or Pt layers by the sputtering technique is extremely large. This benefits the adsorption of the reactant as well as the CO, and thus it enhances the CO poisoning rate. Accordingly, the CO tolerance for the MEAs with a catalyst layer composed of deposited nano Ru/Pt or Pt layer is not as good as that of the catalyst layer with nano Pt–Ru particles inclusive in the carbon. Therefore, we combined the deposited nano Ru/Pt layer with the characteristic of instant CO adsorption and the Pt_{50}–Ru_{50}/C catalyst layer with the best CO tolerance to form the outer catalyst anode layer of IV MEA, hoping to "filter out" CO from the incoming fuel. By combining these two catalyst layers, the "filtration" of CO is expected to be fast and efficient. The resulting fuel entering the inner side of the catalyst layer is free of CO and the direct-printing Pt layer on PEM can normally process the oxidation reaction with hydrogen. The excellent results of the IV MEA in CO tolerance and cell performance, confirm the above inference.

In order to reconfirm, we prepared a new MEA consisting of direct-printing Pt catalyst layer on PEM the same as those for the IV MEA. The anode loading was 0.07 mg cm^{-2} and the cathode loading was 0.25 mg cm^{-2}. This MEA was tested in pure hydrogen fuel to obtain the electrode performance. The polarization curves obtained with various backing pressures for this new MEA are shown in Fig. 13 (at the cell temperature of 65 °C). The current densities obtained at the backing pressures of 100 and 0 kPa were 480.1 and 400.0 mA cm^{-2} at 0.60 V, respectively. The magnitudes of current density are almost same as that of the IV MEA (Fig. 8) at the same operating cell temperature and backing pressures. This suggests that the inner direct-printing Pt catalyst layer at the CO containing hydrogen fuel contributes mostly to the performance of the IV MEA. The only condition for the pure Pt catalyst to process the oxidation reaction is that this Pt catalyst has not been poisoned. Therefore, this indirectly proves the outer catalyst layer consisting of a deposited nano Ru/Pt layer and a screen-printed Pt_{50}–Ru_{50} layer on the GDL efficiently filter out the CO. The fuel entering the inner catalyst layer is thus free of CO.

In order to clarify the filtering effect of the outer catalyst layer, we prepared another new MEA (denoted as V MEA) with an anode structure similar to that of the IV MEA (as shown in Fig. 14). The only difference is the second layer at the outer catalyst layer, i.e. a deposited nano Ru/Pt layer rather than a printing Pt_{50}–Ru_{50} layer. The loadings of each layer at the anode for these two MEAs are identical. This V MEA was tested in hydrogen fuel containing 50 ppm CO to obtain the electrode performance variation with respect to time. Fig. 15 presents the polarization curves as a function of time for the V MEA at 65 °C (cell temperature) and 100 kPa (backing pressure). The performance declined drastically to 21.8 and 96% of the MEA running on pure

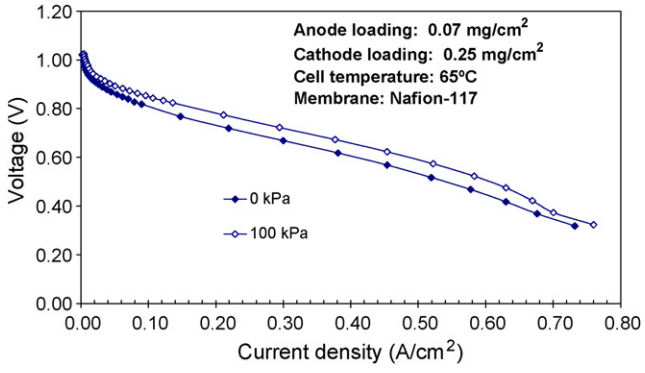

Fig. 13. Polarization curves for various backing pressures for the direct-printed Pt catalyst layer MEA at a cell temperature of 65 °C.

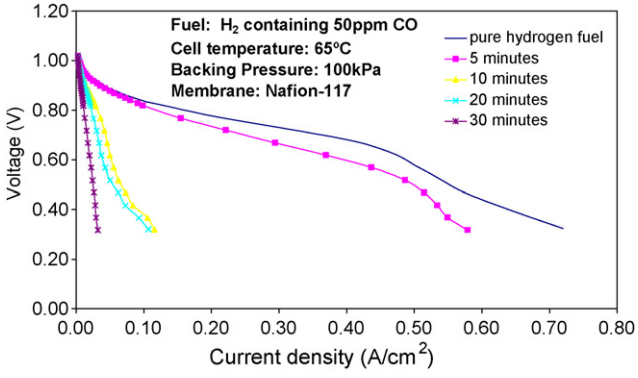

Fig. 15. Variation with time for V MEA when using H_2 containing 50 ppm CO fuel at 65 °C (cell temperature) and 100 kPa (backing pressure).

hydrogen fuel for 5 and 10 min, respectively. The corresponding current densities for 5 and 10 min were 380.3 and 0.06 mA cm^{-2} (at 0.60 V), respectively. This implies that the outer catalyst layer with two deposited nano Ru/Pt layers had poorer tolerance to CO than that of the catalyst layer consisting of a single deposited nano Ru/Pt layer and a printed Pt_{50}–Ru_{50} layer in the hydrogen fuel containing 50 ppm CO. This is because the deposited nano Ru/Pt layer functions as the separator or physical/chemical adsorption of CO from hydrogen as well as reacting with CO to form CO_2 at the Ru:Pt interface. Due to the comparatively small amount of the Ru:Pt interface, the modified electrode would not work after 10 min when the adsorption of CO on Ru/Pt was saturated. By contrast, the anode of IV MEA, whose outer catalyst layer is comprised of a deposited nano Ru/Pt layer and a printed Pt_{50}–Ru_{50} layer, works normally after the adsorption of CO on Ru/Pt is saturated (Fig. 8). This is because the excess CO reacts with Pt_{50}–Ru_{50} second layer of the outer catalyst layer to form CO_2. Therefore, the outer catalyst layer of proposed electrode acts as a CO barrier, and the electrocatalyst Pt/C maintains a high degree of hydrogen oxidation reaction activity even though the platinum loading is low in the inner catalyst layer.

Comparing the results of the proposed anode catalyst layer structure to that of the structure proposed by Huag et al. [18], we believe that the addition of a screen-printing Pt_{50}–Ru_{50} layer on the deposited nano Ru/Pt layer has better CO tolerance than the structure having only the deposited Ru layer in the oxygen free hydrogen containing 50 ppm CO fuel. This increases the safety and fuel utilization. Comparing our results to that of the composite anode prepared by Yu et al. [19], we find that the addition of a deposited nano Ru/Pt layer on the screen-printing Pt_{50}–Ru_{50} layer can lead to a reduced noble metal loading of 0.16 mg cm^{-2} to attain the required CO tolerance ability in the hydrogen containing 50 ppm CO fuel. The enhancement of the utilization efficiency of catalyst may be attributed to the high exposure and extremely large surface area as well as the special electron structure presented by the deposited nano Ru/Pt layer.

4. Conclusions

Our nano Ru/Pt catalyst electrode has shown a high performance and utilization efficiency of the catalyst as well as a comparatively better CO tolerance compared to that of the nano Pt catalyst. This is attributed to the following three reasons: (1) the existence of a Ru:Pt alloy at the interface between the Ru and Pt layers; (2) high exposure and extremely large surface area; (3) special electron structure on the surface of the deposited nano Ru/Pt layer. A combination of this deposited nano Ru/Pt layer with a printed Pt_{50}–Ru_{50} layer to form the outer catalyst layer for the anode electrode provides superior CO tolerance to that of conventional and Huag's [18] structures in CO containing hydrogen fuels. The deposited nano Ru/Pt layer functions as the separator or physical/chemical adsorption "filter" of CO from hydrogen. In addition, it also reacts with CO to form CO_2 at the Ru:Pt interface. The excess CO completely transforms to CO_2 at the Pt_{50}–Ru_{50} second layer of the outer catalyst. The fuel entering the inner catalyst layer is thus free of CO. The inner direct-printing Pt catalyst layer can thus maintain a high activity for the hydrogen oxidation reaction. This means that, by combining a deposited nano Ru/Pt layer and a Pt_{50}–Ru_{50} layer on the GDL acting as a CO barrier with an inner catalyst layer with pure Pt catalyst on PEM, we can obtain an MEA with a high CO tolerance and performance as well as a low noble metal loading. This proposed composite MEA is expected to have an advantage for mass production.

Acknowledgment

The authors are indebted to the National Science Council of Republic of China for financial support of this work (NSC 92-2212-E-451-001).

References

[1] G.J.K. Acres, G.A. Hards, R.J. Potter, T.R. Ralph, D. Thompsett, G.T. Burstein, G.J. Hutchings, Catal. Today 38 (1997) 393.
[2] H. Gasteiger, N.M. Markovic, P.N. Ross, J. Phys. Chem. 99 (1995) 8945.
[3] H. Gasteiger, N.M. Markovic, P.N. Ross, J. Phys. Chem. 99 (1995) 16757.
[4] B.N. Grgur, G. Zhuang, N.M. Markovic, P.N. Ross, J. Phys. Chem. B 100 (1997) 19538.
[5] J.M. Rheaume, B. Muller, M. Schulze, J. Power Sources 76 (1998) 60.
[6] S.J. Lee, S. Mukerjee, E.A. Ticianelli, J. McBreen, Electrochim. Acta 44 (1999) 3283.
[7] B. Rohland, V. Plzak, J. Power Sources 84 (1999) 183.
[8] S. Mukerjee, S.J. Lee, E.A. Ticianelli, J. McBreen, B.N. Grgur, N.M. Markovic, P.N. Ross, J.R. Giallombardo, E.S. De Castro, Electrochem. Solid State Lett. 2 (1999) 12.
[9] B.N. Grgur, N.M. Markovic, P.N. Ross, J. Electrochem. Soc. 146 (1999) 1613.
[10] K.Y. Chen, Z. Sun, A.C.C. Tseung, Electrochem. Solid State Lett. 3 (2000) 10.
[11] P. Gouerec, M.C. Denis, D. Guay, J.P. Dodelet, R. Schulz, J. Electrochem. Soc. 147 (2000) 3989.
[12] A. Pozio, L. Giorgi, E. Antolini, E. Passalacqua, Electrochim. Acta 46 (2000) 555.
[13] T.J. Schmidt, Z. Jusys, H.A. Gasteiger, R.J. Behm, U. Endruschat, H. Boennemann, J. Electroanal. Chem. 501 (2001) 132.
[14] S. Gottesfeld, US Patent 4,910,099 (1990).
[15] S. Gottesfeld, J. Pafford, J. Electrochem. Soc. 135 (1998) 2651.
[16] R.J. Bellows, E. Marucchi-Soos, R.P. Reynolds, Electrochem. Solid State Lett. 1 (1998) 69.
[17] A. Huag, R.E. White, J.W. Weidner, W. Huang, J. Electrochem. Soc. 149 (2002) A862.
[18] A. Huag, R.E. White, J.W. Weidner, W. Huang, S. Shi, N. Rana, S. Grunow, T.C. Stoner, A.E. Kaloyeros, J. Electrochem. Soc. 149 (2002) A868.
[19] H.M. Yu, Z.J. Hou, B.I. Yi, Z.Y. Lin, J. Power Sources 105 (2002) 52.
[20] C.C. Hsu, C.C. Wan, J. Power Sources 115 (2003) 268.
[21] S.J. Lee, S. Murkerjee, J. McBreen, Y.W. Rho, Y.T. Kho, T.H. Lee, Electrochim. Acta 43 (1998) 3693.
[22] R.L. Borup, N.E. Vanderborgh, Electrochem. Soc. Proc. 95 (23) (1995) 167.
[23] N. Fujiwara, K. Yasuda, T. Ioroi, Z. Siroma, Y. Miyazaki, Electrochim. Acta 47 (2002) 4079.
[24] T. Biegler, D.A.J. Rand, R. Woods, J. Electroanal. Chem. 29 (1971) 269.